REPORT DOCUMENTATION PAGE

Form Approved OMB NO. 0704-0188

1. REPORT DATE (DD-MM-YYYY)	2. REPORT TYPE	3. DATES COVERED (From - To)
23-06-2015	Final Report	1-Oct-2011 - 31-Mar-2015

4. TITLE AND SUBTITLE
Final Report: Nonlinear Corrections to Temperature in Computer Simulations of Complex Systems

5a. CONTRACT NUMBER
W911NF-11-1-0419

5b. GRANT NUMBER

5c. PROGRAM ELEMENT NUMBER
611102

6. AUTHORS
Ralph V. Chamberlin

5d. PROJECT NUMBER

5e. TASK NUMBER

5f. WORK UNIT NUMBER

7. PERFORMING ORGANIZATION NAMES AND ADDRESSES
Arizona State University
P.O. Box 876011

Tempe, AZ 85287 -6011

8. PERFORMING ORGANIZATION REPORT NUMBER

9. SPONSORING/MONITORING AGENCY NAME(S) AND ADDRESS (ES)
U.S. Army Research Office
P.O. Box 12211
Research Triangle Park, NC 27709-2211

10. SPONSOR/MONITOR'S ACRONYM(S)
ARO

11. SPONSOR/MONITOR'S REPORT NUMBER(S)
59435-EG.9

12. DISTRIBUTION AVAILIBILITY STATEMENT
Approved for Public Release; Distribution Unlimited

13. SUPPLEMENTARY NOTES
The views, opinions and/or findings contained in this report are those of the author(s) and should not contrued as an official Department of the Army position, policy or decision, unless so designated by other documentation.

14. ABSTRACT
Temperature is the familiar thermodynamic quantity that governs heat flow between large systems. However, temperature comes from just the linear (first-order) derivative of entropy with respect to energy, so that nonlinear corrections may contribute significantly to the equilibrium properties of small systems. Moreover, the nonlinear corrections also influence the thermal and dynamic properties of independently-relaxing nanometer-sized regions ("hot spots") inside bulk materials. Several experimental techniques have shown that such localized regions dominate the primary response of most materials. During the grant period we have greatly extended our

15. SUBJECT TERMS
hot spots, local temperature, finite-size effects in computer simulations, 1/f noise, nanothermodynamics, maximum entropy

16. SECURITY CLASSIFICATION OF:			17. LIMITATION OF ABSTRACT	15. NUMBER OF PAGES	19a. NAME OF RESPONSIBLE PERSON
a. REPORT	b. ABSTRACT	c. THIS PAGE			Ralph Chamberlin
UU	UU	UU	UU		19b. TELEPHONE NUMBER 480-965-3922

Report Title

Final Report: Nonlinear Corrections to Temperature in Computer Simulations of Complex Systems

ABSTRACT

Temperature is the familiar thermodynamic quantity that governs heat flow between large systems. However, temperature comes from just the linear (first-order) derivative of entropy with respect to energy, so that nonlinear corrections may contribute significantly to the equilibrium properties of small systems. Moreover, the nonlinear corrections also influence the thermal and dynamic properties of independently-relaxing nanometer-sized regions ("hot spots") inside bulk materials. Several experimental techniques have shown that such localized regions dominate the primary response of most materials. During the grant period we have greatly extended our fundamental understanding of these regions, and can now simulate several of their properties. This Final Report describes our key findings, with an emphasis on comparing computer simulations to experimental data.

Enter List of papers submitted or published that acknowledge ARO support from the start of the project to the date of this printing. List the papers, including journal references, in the following categories:

(a) Papers published in peer-reviewed journals (N/A for none)

Received		Paper
02/27/2013	3.00	T. Kim, R. V. Chamberlin, J. P. Bird. Large Magnetoresistance of Nickel-Silicide Nanowires: Non-Equilibrium Heating of Magnetically-Coupled Dangling Bonds, Nano Letters, (02 2013): 0. doi: 10.1021/nl3044585
04/20/2015	8.00	Ralph Chamberlin. The Big World of Nanothermodynamics, Entropy, (12 2014): 52. doi: 10.3390/e17010052
11/17/2014	1.00	Ralph V. Chamberlin. Monte Carlo simulations including energy from an entropic force, Physica A: Statistical Mechanics and its Applications, (11 2012): 5384. doi: 10.1016/j.physa.2012.06.016
11/18/2014	6.00	Ralph V. Chamberlin, Derek M. Nasir. 1/f noise from the laws of thermodynamics for finite-size fluctuations, Physical Review E, (07 2014): 12142. doi: 10.1103/PhysRevE.90.012142
11/19/2014	7.00	Ralph V. Chamberlin, Bryce F. Davis. Modified Bose-Einstein and Fermi-Dirac statistics if excitations are localized on an intermediate length scale: Applications to non-Debye specific heat, Physical Review E, (10 2013): 42108. doi: 10.1103/PhysRevE.88.042108
TOTAL:	**5**	

Number of Papers published in peer-reviewed journals:

(b) Papers published in non-peer-reviewed journals (N/A for none)

Received	Paper

TOTAL:

Number of Papers published in non peer-reviewed journals:

(c) Presentations

Adapting Monte Carlo simulations to obey the laws of thermodynamics on intermediate lengths
Gordon Research Conference on Energetic Materials, Sunday River, Maine, June 18, 2014

Number of Presentations: 1.00

Non Peer-Reviewed Conference Proceeding publications (other than abstracts):

Received	Paper	
08/28/2013	5.00	Ralph V. Chamberlin, Pierre Gaspard, Debra J. Searles. EQUILIBRIUM AND NON-EQUILIBRIUM FLUCTUATIONS IN SMALL-SYSTEM THERMODYNAMICS, 12th Joint European Thermodynamics Conference 2013. 03-JUL-13, . : ,

TOTAL: **1**

Number of Non Peer-Reviewed Conference Proceeding publications (other than abstracts):

Peer-Reviewed Conference Proceeding publications (other than abstracts):

Received	Paper

TOTAL:

Number of Peer-Reviewed Conference Proceeding publications (other than abstracts):

(d) Manuscripts

Received	Paper	
08/28/2013	4.00	Bryce F. Davis, Ralph V. Chamberlin. Modified Bose-Einstein and Fermi-Dirac statistics if excitations are localized on an intermediate length scale: Application to non-Debye specific heat , Submitted to physical review E (07 2013)
TOTAL:	**1**	

Number of Manuscripts:

Books

Received	Book
TOTAL:	

Received	Book Chapter
TOTAL:	

Patents Submitted

Patents Awarded

Awards

Invited speaker: Gordon Research Conference on Energetic Materials, Sunday River, Maine, June 2014

Graduate Students

NAME	PERCENT_SUPPORTED	Discipline
Shane Moffet	0.20	
Bryce Davis	0.20	
Andrew Shevchuk	0.05	
FTE Equivalent:	**0.45**	
Total Number:	**3**	

Names of Post Doctorates

NAME	PERCENT_SUPPORTED
FTE Equivalent:	
Total Number:	

Names of Faculty Supported

NAME	PERCENT_SUPPORTED	National Academy Member
Ralph V. Chamberlin	0.10	
FTE Equivalent:	**0.10**	
Total Number:	**1**	

Names of Under Graduate students supported

NAME	PERCENT_SUPPORTED	Discipline
Alexander Brown	0.10	Physics
Derek Nasir	0.10	Physics
FTE Equivalent:	**0.20**	
Total Number:	**2**	

Student Metrics

This section only applies to graduating undergraduates supported by this agreement in this reporting period

The number of undergraduates funded by this agreement who graduated during this period: 2.00

The number of undergraduates funded by this agreement who graduated during this period with a degree in science, mathematics, engineering, or technology fields:..... 2.00

The number of undergraduates funded by your agreement who graduated during this period and will continue to pursue a graduate or Ph.D. degree in science, mathematics, engineering, or technology fields:..... 1.00

Number of graduating undergraduates who achieved a 3.5 GPA to 4.0 (4.0 max scale):..... 1.00

Number of graduating undergraduates funded by a DoD funded Center of Excellence grant for Education, Research and Engineering:..... 0.00

The number of undergraduates funded by your agreement who graduated during this period and intend to work for the Department of Defense 0.00

The number of undergraduates funded by your agreement who graduated during this period and will receive scholarships or fellowships for further studies in science, mathematics, engineering or technology fields:..... 0.00

Names of Personnel receiving masters degrees

NAME

Total Number:

Names of personnel receiving PHDs

NAME

Total Number:

Names of other research staff

NAME PERCENT_SUPPORTED

FTE Equivalent:
Total Number:

Sub Contractors (DD882)

Inventions (DD882)

Scientific Progress

See Attachment

Technology Transfer

In July of 2014, I visited the Multiscale Reactive Modeling Team of Dr. Betsy Rice at the US Army Research Laboratory. I gave a presentation describing our recent work. We had extensive discussions regarding some key issues in simulating energetic materials. We have submitted a Cooperative Agreement to strengthen and expand our collaboration.

FINAL REPORT

Nonlinear Corrections to Temperature in Computer Simulations of Complex Systems

Proposal: 59435-EG: DOD-Army Research Office
Sponsor Agreement Number: W911NF-11-1-0419

Dates: 10/01/2011-03/30/2015

Program Manager: Ralph A. Anthenien Jr, PhD, PE
Propulsion & Energetics
U.S. Army Research Office
P.O. Box 12211
Research Triangle Park, NC 27709-2211
ralph.anthenien1@us.army.mil

Principal Investigator: Ralph V. Chamberlin, PhD
Department of Physics
Arizona State University
Tempe, AZ 85287-1504
Phone: (480) 965-3922
Fax: (480) 965-7954
ralph.chamberlin@asu.edu

Nonlinear Corrections to Temperature in Computer Simulations of Complex Systems

Abstract

Temperature is the familiar thermodynamic quantity that governs heat flow between large systems. However, temperature comes from just the linear (first-order) derivative of entropy with respect to energy, so that nonlinear corrections may contribute significantly to the equilibrium properties of small systems. Moreover, the nonlinear corrections also influence the thermal and dynamic properties of independently-relaxing nanometer-sized regions ("hot spots") inside bulk materials. Several experimental techniques have shown that such localized regions dominate the primary response of most materials. During the grant period we have greatly extended our fundamental understanding of these regions, and can now simulate several of their properties. This Final Report describes our key findings, with an emphasis on comparing computer simulations to experimental data.

Foreword

Most of the results presented here come from Monte Carlo (MC) simulations of the Ising model. The first nonlinear correction we found allows simulations that exhibit extensive thermal fluctuations, consistent with measured heat capacity and usual definitions of extensive entropy. Furthermore, this correction significantly improves the agreement between the Ising model and measured non-classical scaling behavior of ferromagnetic materials and critical fluids. A related nonlinear correction yields spectra that exhibit $1/f$-like noise, providing a fundamental mechanism for the low-frequency thermal fluctuations exhibited by most materials. Indeed these corrections give a unified picture for several empirical laws, including commonly measured deviations from the mathematical formulas. A simplified Creutz model is found that requires two types of nonlinear corrections to temperature. The model consists of a spin system coupled to an explicit heat bath. One mismatch in temperature comes from finite-size effects in the heat bath, while the second mismatch arises if excitations in the heat bath are localized on an intermediate length. Results from this model give good agreement with the excess specific heat of imperfect crystals at low temperatures. Another model, which involves adiabatic demagnetization with weak coupling to the heat bath, describes measurements of time-dependent magnetoresistance in nanowires at low temperatures. Recently we have found that fluctuations in molecular-dynamics (MD) simulations of dilute systems at low temperatures deviate from the equipartition theorem. We are currently searching for the optimal nonlinear corrections for these MD simulations, so that they may also yield improved agreement with thermodynamic behavior and with experiments, similar to the corrections we have found for MC simulations. The fundamental goal of our research is to fully understand finite-size thermal effects inside complex materials, with a practical result of improved accuracy, efficiency, and predictive power of computer simulations.

TABLE OF CONTENTS

1. Introduction [1]

Temperature is the primary thermodynamic quantity that governs the equilibrium of systems in thermal contact with a heat bath. Ideally, the heat bath must be homogeneous and effectively infinite, while the coupling to the system must be weak, so that the bath changes only from heat exchange with the system. We have investigated some consequences of small thermal baths, with strong coupling to the system. We are guided by the theory of small-system thermodynamics, introduced by Hill in 1962 [2,3], which establishes the fundamental laws that govern finite-size effects in thermodynamics. Although originally developed to describe individual molecules and isolated nanoparticles, we use this "nanothermodynamics" for treating the heterogeneous distribution of independently relaxing regions inside bulk materials. Several experimental techniques have shown that such nanometer-sized regions dominate the primary response of most materials [4-9].

We use two key concepts from nanothermodynamics: Hill's subdivision potential (E) and the fully-open nanocanonical ensemble. The nanocanonical ensemble facilitates systematic treatment of independently-relaxing regions in thermal contact with an ensemble of similar regions, consistent with the primary response of most materials. Other ensembles impose artificial internal constraints on the regions, as shown schematically in Fig. (1). In general, the distribution of internal region sizes is governed by Hill's E. Furthermore, this E must be included in the 1st law of thermodynamics if total energy is to be conserved [10]. Hill's E can be understood by comparison to Gibbs' chemical potential, μ. μ is the change in energy to take a single particle from a bath of particles into the system, whereas E is the change in energy to take a cluster of n interacting particles from a bath of clusters into the system, and in general n interacting particles do not have the same energy as n isolated particles due to surface terms, length-scale effects, thermal fluctuations, etc. Thus, E is needed to systematically treat the nonlinear and non-

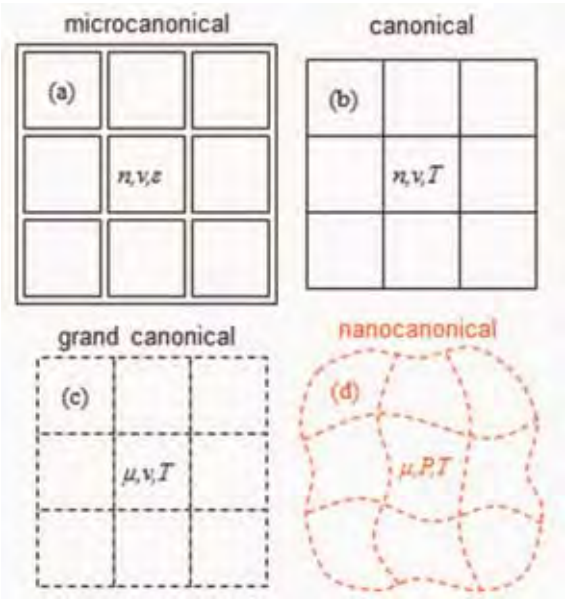

Figure 1. From Ref. [12]. Various ensembles for fluctuations inside a bulk sample. The microcanonical ensemble applies to fully-closed fluctuations that conserve number of particles (n), volume (v), and energy (ε). The canonical ensemble (n,v,T) applies to fluctuations at constant volume when only heat flows in and out from the rest of the sample. The grand canonical ensemble (μ,v,T) applies to fluctuations at constant volume when particles also flow in and out from the rest of the sample. The "nanocanonical" ensemble (μ,P,T) applies to fully-open fluctuations, where the volume of the fluctuation is allowed to change as particles flow in and out.

extensive contributions to energy from a system that contains a heterogeneous distribution of independent regions. Moreover, $E \rightarrow 0$ governs the distribution of regions if their sizes are not fixed, similar to how $\mu \rightarrow 0$ governs the distribution of particles if their numbers are not fixed.

We have used the concepts of nanothermodynamics as a guide to treat independent thermal fluctuations inside bulk samples. We find that the resulting models and theories yield improved agreement with the measured response of many materials [11-17]. Indeed, these concepts provide a physical explanation for several empirical formulas that are used to characterize the complex dynamics of realistic materials. In fact we have shown that nanothermodynamics provides a fundamental basis for: non-exponential relaxation, non-Arrhenius activation, non-classical critical scaling, non-homogeneous response, and non-Nyquist noise, including most-often observed deviations from the simple empirical formulas. First I will describe our recent success in finding a physical foundation for thermal fluctuations that yield non-Nyquist noise.

2. Non-Nyquist Noise

Nature exhibits several types of noise due to thermal fluctuations [18]. In 1827, Brown first reported sporadic motion of pollen grains in water. In 1905, as the second breakthrough in his *Annus Mirabilis*, Einstein explained this "Brownian motion" by assuming random impulses from much smaller particles, which was to provide the first definitive evidence for atoms and molecules. As a function of frequency (f) Brownian motion exhibits noise with a power spectral density that varies as $S(f) \propto 1/f^2$. In 1926 Johnson first measured electronic noise that showed a flat spectral density, $S(f)$ = const. Nyquist explained this "white" noise by assuming classical thermal fluctuations in the motion of the electrons. Also in 1926 Johnson measured electronic noise with apparent $1/f$ frequency dependence. Although there is still no widely accepted explanation for this "$1/f$ noise," empirically it is the most common low-frequency behavior. Indeed $1/f$ noise is found in metals, semimetals, semiconductors, dielectrics, ferroelectrics, ionic conductors, spin glasses, supercooled liquids, and quantum devices [19-22], as well as in music, speech, neural response, and human perception [23-26]. Although no single model is likely to explain all these phenomena, the laws of nanothermodynamics provide a unified picture for $1/f$ noise in many materials. Specifically, the general principle is based on the assumption that particles inside local regions of a bulk sample: conserve total energy by including non-extensive terms in E (1^{st} law), maintain maximum entropy during equilibrium fluctuations (2^{nd} law), and/or exhibit statistical indistinguishability of identical particles consistent with quantum mechanics, as described below.

3. Computer Simulations of the Ising model

Most simulations presented here utilize the Ising model for binary degrees of freedom ("spins") on a simple-cubic lattice. The lattice contains a total of N spins, with exchange interaction (J) between nearest-neighbor spins, and periodic boundary conditions between the outside surfaces of the lattice. Often the lattice is subdivided into smaller regions containing $n <$

N spins to study the thermal properties of small systems inside a bulk sample. Figure 2 (a) shows the net magnetization as a function of time from simulations of this model. Note the abrupt change in dynamics at time $t = 0$: for $t < 0$ the spin-flip probability is governed by Boltzmann's factor alone using the Metropolis algorithm Eq. (1), whereas for $t \geq 0$ there is also a nonlinear correction from nanothermodynamics Eq. (2).

$$e^{-\Delta U/k_B T} > rand[0,1) \quad \text{Boltzmann Factor} \tag{1}$$

$$e^{g(S_m - S_0)/k_B} > rand[0,1) \quad \text{Nonlinear Correction} \tag{2}$$

In Eq. (1), ΔU is the change in interaction energy, k_B is Boltzmann's constant, and T is temperature. In Eq. (2), g controls the strength of the nonlinear correction, which comes from the alignment entropy using the binomial coefficient for binary degrees of freedom: $S_m / k_B = \ln \frac{n!}{[\frac{1}{2}(n+m)]![\frac{1}{2}(n-m)]!}$, with $S_0 / k_B = \ln \frac{n!}{[(\frac{1}{2}n)!]^2}$ its maximum value. When $g = 0$ ($t<0$ in Fig. 2 (a)) systems of all size show standard Gaussian fluctuations characteristic of white noise (see Fig. 3). When $g=1$ ($t \geq 0$) the uppermost set of data (from a large lattice with small regions) shows large wandering on all time scales, indicative of $1/f$ noise (see Fig. 3); while the lower two sets of data (from smaller lattices that contain a single region) exhibit sharp jumps and steps characteristic of non-Gaussian fluctuations. Furthermore, Fig. 2 (b) shows that histograms of the simulations exhibit trimodal behavior (symbols), similar to the trimodal behavior found from measurements of $1/f$ noise in a spin glass and ionic conduction through a nanopore, shown in the upper part of Fig. 2 (b) (solid lines). In contrast, the bottom pair of lines, from fluctuations in two different double-well potentials, shows simpler bimodal behavior.

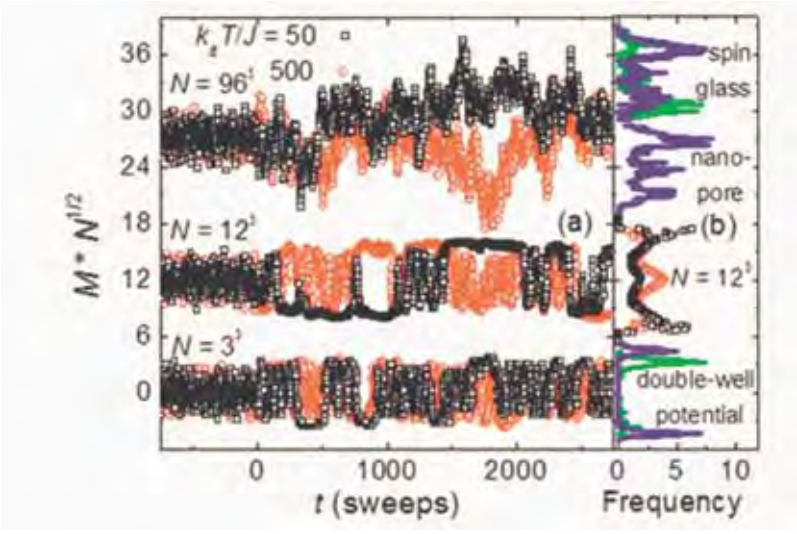

Figure 2. From Ref. [17]. **(a)** Scaled magnetization versus time at two temperatures, from simulations of the Ising model. Note that simulations from lattices with different sizes, *N*, are offset for clarity. The dynamics changes abruptly at $t = 0$ when a nonlinear correction (Eq. (2)) is included with Boltzmann's factor (Eq. (1)). **(b)** Histograms of the simulations from $N = 12$ (symbols) and from the noise measured in three types of samples (solid lines). Note the trimodal behavior from the simulations, spin glass, and nanopore system.

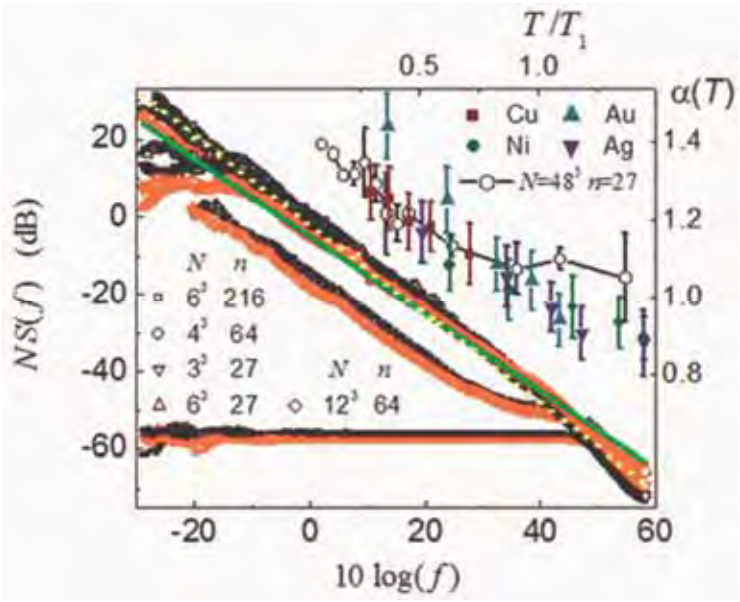

Figure 3. From Ref. [17]. Left side shows frequency dependence of noise from simulations at k_BT/J=50 and 500, similar to those in Fig. 2. $S(f)$ is multiplied by N to scale different lattice sizes (given in the legend) and $\log(f)$ is multiplied by 10 to match the dB scale. The spectra exhibiting white noise (bottom) come from using Eq. (1) alone. Spectra exhibiting $1/f$–like behavior (diagonal) come from the same model using both Eq. (1) and Eq. (2). Over a broad range of frequencies these simulations can be characterized by $S(f) \propto 1/f^{\alpha(T)}$, with $\alpha(T) \approx 1.0$ for k_BT/J=500 (solid line) and $\alpha(T) \approx 1.15$ for k_BT/J=50 (dotted line). Diamond-shaped symbols, which show $1/f$ noise at low frequencies and white noise at higher frequencies, come from a heterogeneous system. Right side of figure shows $\alpha(T)$ from measurements on various metallic thin-films (solid symbols) and simulations (open hexagons connected by solid lines). Note that the temperatures are normalized by T_1, where $\alpha(T)$ extrapolates to 1.

The left side of Fig. 3 shows the Fourier transform from simulations similar to those in Fig. 2 (a). Simulations using Eq. (1) alone yield white noise that does not depend on f (lower symbols), whereas adding Eq. (2) yields $1/f$-like noise (symbols along the diagonal). In fact these simulations can be characterized by $S(f) \propto 1/f^{\alpha(T)}$, with a temperature-dependent spectral-density exponent $\alpha(T)$ that is consistent with the measured behavior from several metals at lower temperatures, as shown in the upper corner of Fig. 3. Similar large-amplitude low-frequency noise is found in most substances. Thus, Eq. (2) provides a formula for obtaining measured $1/f$-like noise, including deviations from pure $1/f$-behavior. Moreover, the nonlinear correction is based on strict adherence to the fundamental laws of thermodynamics, as described below.

Figure 4 depicts some of the mechanisms that justify the nonlinear correction. Consider two binary degrees of freedom, e.g. two uniaxial spins that can be up or down. Figure 4 (a) shows that there is one way to have both spins up, one way to have both spins down, and two ways to have no net alignment. The alignment entropy is obtained from Boltzmann's definition, $S/k_B = \ln(\Omega)$, using the multiplicity of each alignment, Ω. The dashed (blue) line in Fig. 4 (b) shows how, during normal thermal fluctuations, this entropy may fluctuate up-and-down between its maximum $S/k_B = \ln(2)$ and minimum $S/k_B = 0$ values. Although seeming to violate the 2nd law of thermodynamics, various explanations have been proposed. First: the entropy of small system may decrease temporarily, which is the usual assumption of various fluctuation theorems [27]; but clear violations of the 2nd law require completely-closed systems, which cannot be measured. Second: entropy could be defined using Gibbs ensembles that average over all available states, but this inhibits using entropy for time-dependent and out-of-equilibrium behavior. A third

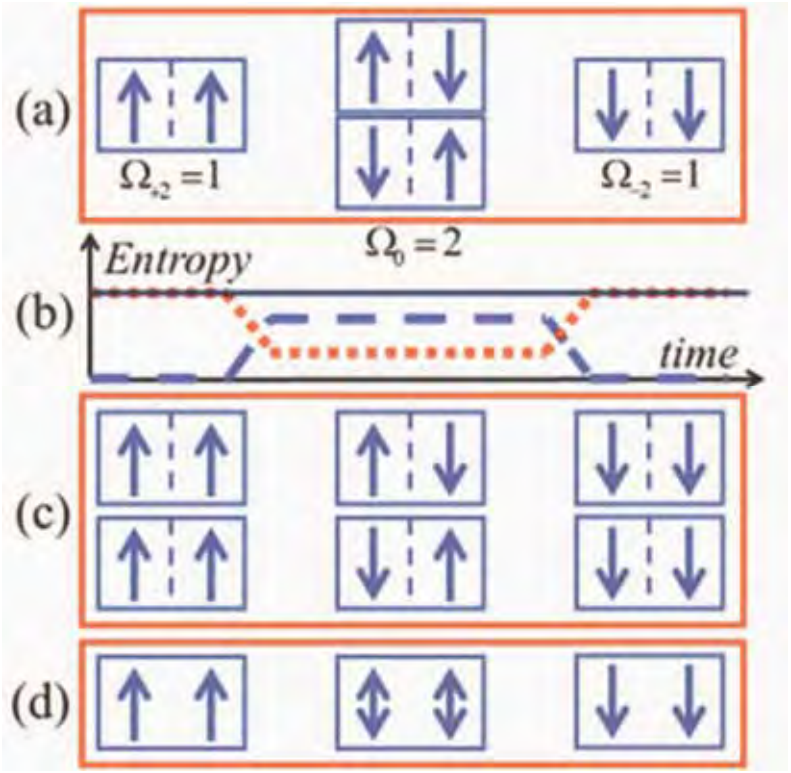

Figure 4. From Ref. [17]. (**a**) Sketch of possible states in a region containing two binary spins. (a) For distinguishable spins there is one way to have both up ($\Omega_{+2}=1$) or down ($\Omega_{-2}=1$), but two ways to have zero net alignment ($\Omega_0=2$). **(b)** During thermal fluctuations the Boltzmann entropy of the spins goes up and down (dashed line). To maintain maximum entropy the entropy of a bath must go down and up (dotted line), so that the combined entropy of the system plus bath is constant (solid line). **(c)** When the bath has high entropy each low-entropy state in the region persists twice as long as expected from the Boltzmann factor alone. **(d)** Alternatively, zero alignment may come from a single state that contains a superposition of spins, consistent with de-localized particles that are indistinguishable in the region.

possibility is that when the entropy of a local region decreases, the entropy of its bath increases, so that the total entropy remains maximized. Indeed, Fig. 4 (b) shows how the entropy of the bath (dotted line) may balance the entropy of the system (dashed line), so that the combined entropy of the system plus bath is constant (solid line).

This entropy-transfer mechanism for the nonlinear correction comes from a type of entropic force, similar to Boltzmann's factor [16]. Boltzmann's factor favors low-energy states because increasing the energy of the system lowers the entropy of the bath. Similarly, the nonlinear correction favors low-entropy states because increasing the alignment entropy of the system lowers the entropy of the bath. In fact, for the two-spin system the nonlinear correction precisely doubles the average lifetime of each fully aligned state, as shown schematically in Fig. 4 (c). Thus, each aligned state becomes as likely as both unaligned states. Information theory provides additional insight into this mechanism. If there is no transfer of information between the system and its environment, then the alignment of the system cannot be known and its multiplicity always includes all four states. Again the entropy is constant, remaining at the value $S/k_B=\ln(4)$.

A second mechanism for the nonlinear correction comes from the statistics of indistinguishable particles, as shown schematically in Fig. 4 (d). To match the probability of each alignment in Fig. 4 (c), instead of doubling the likelihood of the aligned states, the unaligned state could be a single superposition of up- and down-spins, as expected for identical particles that are subject to the exchange interaction. Indeed, the three net alignments (up, down, and unaligned) form the triplet state of a two-spin system. (The less-likely singlet state is neglected in such a simplistic picture.) Further justification for this interpretation comes from the energy and its fluctuations shown in Fig. 5 (below), where a similar nonlinear correction

minimizes the energy of small regions and makes their entropy extensive and additive, consistent with the statistics of indistinguishable particles. Thus, this mechanism for extensive entropy in small regions is similar to the semi-classical ideal gas that resolves Gibbs' paradox for extensive entropy in large volumes. In other words, the nonlinear correction may be a simplistic way to simulate quantum-like behavior in classical models.

A third way to understand the nonlinear correction is from conservation of energy including Hill's subdivision potential. Consider a system of n non-interacting Ising-like spins with magnetic moment μ_B in field B. Each spin can be aligned or anti-aligned with B, giving energy $-\mu_B B$ or $+\mu_B B$, respectively. The single-particle partition function is $Z_1 = e^{\mu_B B/k_B T} + e^{-\mu_B B/k_B T}$. Because the spins are non-interacting, the partition function for n spins is $Z = (Z_1)^n$, yielding the free energy $A = -nk_B T \ln(Z_1)$. For simplicity let $B \to 0$, so that $A = -nk_B T \ln(2)$. Again using the binomial coefficient for the exact entropy of the system, the internal energy becomes $U_m = A + TS_m = -nk_B T \ln(2) + k_B T \ln \frac{n!}{[\frac{1}{2}(n+m)]![\frac{1}{2}(n-m)]!}$. If the system is at its average alignment m=0, Stirling's approximation for the factorials yields $S_0 / k_B \approx n \ln(2)$ and $U_0 \approx 0$. However, if total energy is to be conserved during fluctuations, there is a non-extensive contribution to internal energy $U_m = U_0 - E_m$, where $E_m = k_B T (S_0 - S_m)$ is Hill's subdivision potential. In other words, although $U_0 \approx 0$ at $m = 0$, during thermal fluctuations the change in alignment entropy causes a change in energy, even if there are no interactions between particles. Fluctuations in E_m occur because free energy is a thermal average over all states, while instantaneous energy and entropy may be defined for every state. Note that when $m \neq 0$, $E_m > 0$ lowers the total energy, which favors subdividing a bulk sample into an ensemble of regions that fluctuate independently to increase the fluctuations, as is found in the primary response of most materials. Inserting this E_m from entropy into a Boltzmann-like factor yields the nonlinear correction, Eq. (2). Interaction energies that appear explicitly in Eq. (1) neglect this source of energy. Thus, Eq. (2) must be included if total energy is to be strictly conserved during equilibrium fluctuations.

Deviations from thermodynamic behavior shown by standard simulations using Eq. (1) alone are due to finite-size effects from assuming homogeneous systems with uniform correlations. Specifically, when energy fluctuations are averaged over a volume that excludes interacting particles outside the volume, correlations across the interface are neglected. For large homogenous systems the nonlinear correction gives a relatively small contribution to conservation of energy: $n \to \infty$ yields $m \to 0$, and $E_0 \approx 0$. However, several experimental techniques have established that the primary response of most materials comes from a heterogeneous distribution of independently-relaxing nanometer-sized regions. Indeed, dynamical heterogeneity in the correlations between regions has been found in the slow response of liquids, glasses, polymers, and crystals [4-9]. In fact, extensive studies of time-dependent specific heat at low temperatures find that the only substance to show no evidence for localized excitations is chemically and isotopically pure NaF crystals [28]. Furthermore, the technique of nonresonant spectral hole burning (NSHB) establishes that excess energy is localized in selected degrees of freedom inside a sample for minutes, or even hours [29,30], without influencing the

energy in neighboring regions. Thus, complexity in the primary response of most substances comes from thermodynamic heterogeneity due to an ensemble of independently relaxing regions, consistent with nanothermodynamics, but different from the behavior assumed for standard thermodynamics.

Energy fluctuations in most Monte Carlo simulations exhibit a size dependence [31] that differs from the expectation that entropy is extensive and additive. Figure 5 shows the average potential energy density ($<U/J>/n$) and its fluctuations ($<(\Delta U/kT)^2>/n$) as a function of the number of particles (n) in local regions of a large lattice. Again the simulations utilize the standard Ising model for binary spins on a simple-cubic lattice with ferromagnetic interaction between nearest-neighbors. The solid (black) lines, from simulations using Boltzmann's factor alone (Eq. (1)), show constant energy density, whereas the fluctuations in energy density increase with increasing region size. The size dependence of these energy fluctuations yields a size-dependent specific heat that is inconsistent with NSHB measurements, while integrating the heat capacity yields non-extensive entropy that is incompatible with standard definitions. The symbols in Fig. 5 show the energy density and its fluctuations for the same Ising model with various strengths (g) in an approximation of Eq. (2) that yields a quadratic correction to Boltzmann's factor, with a bypass.

$$\exp\left[-g\,\tfrac{1}{2}\frac{m^2}{n}(1-\delta_{\Delta U,0})\right] \qquad \text{Quadratic Correction} \tag{3}$$

The bypass comes from the Kronecker delta that gives $(1-\delta_{\Delta U,0}) = 0$ when $\Delta U = 0$. A practical reason for this bypass is to accelerate slow relaxation and avoid frozen response. A physical reason is that if $\Delta U = 0$, spin flips can occur in a microcanonical ensemble without coupling to the heat bath. Sufficient disorder in a local region may remove the bypass if neighboring states with $\Delta U = 0$ are not available, consistent with the fact that $1/f$ noise generally increases with increasing disorder. Furthermore, most materials exhibit a combination of $1/f$ noise at low frequencies and white noise at high frequencies, indicating dynamics without, and with, the bypass, respectively. Indeed, the diamond-shaped symbols in Fig. 3 come from a heterogeneous mixture of Eq. (2) and $e^{(S_m-S_0)(1-\delta_{\Delta U,0})/k_B} > rand[0,1)$. In any case, Figs. 5 (a)-(d) show that increasing g in Eq. (3) reduces the energy density and increases the energy fluctuations per particle, until g=1 where the energy of small regions is minimized and the specific heat is independent of region size. Thus, g=1 yields behavior that is most consistent with thermodynamic equilibrium: energy that is minimized and fluctuations in energy that yield extensive entropy. Empirical evidence for extensive entropy, even in small regions inside bulk samples, comes from the technique of NSHB showing that the specific heat is constant for independently relaxing regions [32], even for very small regions having $n \sim 10$ molecules [33].

Figure 5. From Ref. [14]. Size dependence of (**a**) average energy per particle and **(b)** its fluctuations from MC simulations of the Ising model Solid lines come from using the standard Metropolis algorithm; symbols come from simulations with varying strength of a nonlinear correction, with g=1 the expected correction from a Taylor series expansion of entropy. The dashed lines show that g=1 yields energy reductions proportional to 1/n in (a), and constant energy fluctuations in (b). **(c)** Average energy per particle, and **(d)** its fluctuations, as a function of the strength of the nonlinear correction. Each type of symbol comes from a different region size, as given in the legend.

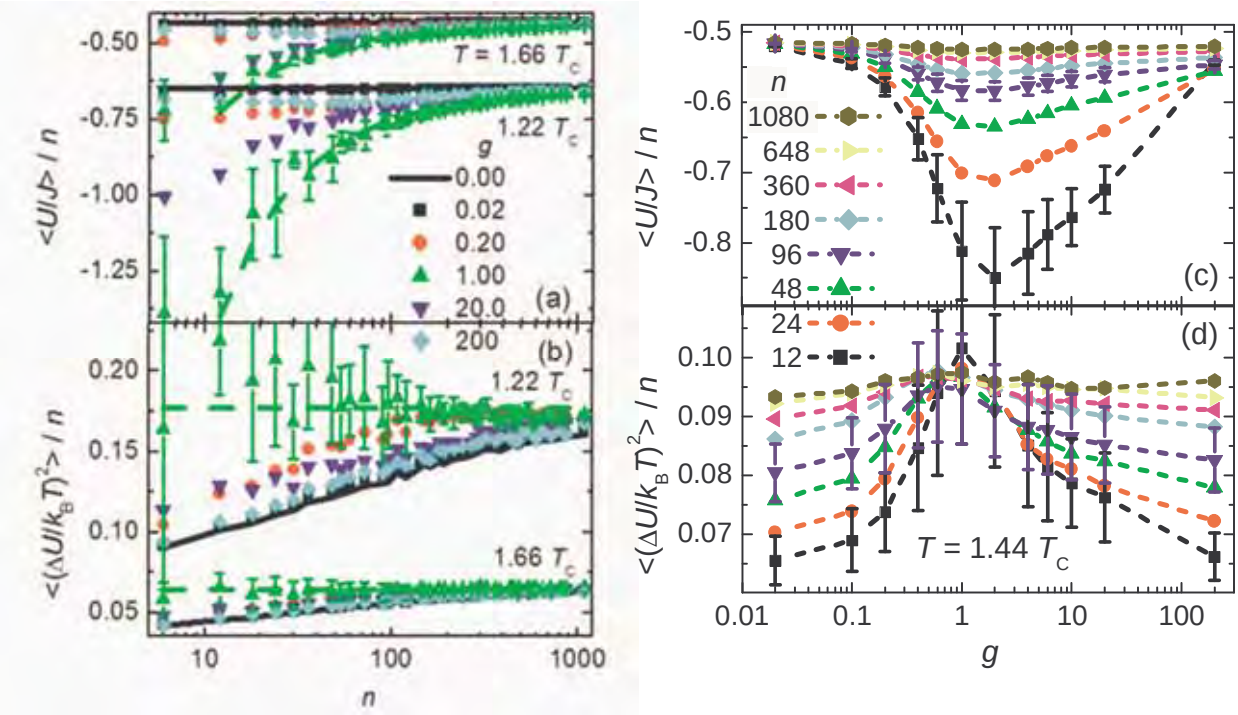

4. Comparison of Computer Simulations with Measurements

The nonlinear correction also improves agreement between computer simulations and the measured response of many materials. The symbols in Fig. 6 (a) show the magnetic susceptibility from single-crystal gadolinium as a function of reduced temperature. At high temperatures the data have a slope of –1.0, consistent with the Curie-Weiss law. As $T \rightarrow T_C$ the red (dashed) line approaches a constant slope of –1.24, showing that standard simulations of the Ising model using Boltzmann's factor alone are consistent with renormalization group theory for homogeneous samples in the canonical ensemble. However, close inspection of the data reveals that the slope is not constant as $T \rightarrow T_C$. The solid (black) curve in Fig. 6 (a), which shows improved agreement with the data at all temperatures, comes from simulations of the same Ising model with the quadratic correction (g=1 in Eq. (3)) expected for heterogeneous systems obeying nanothermodynamics. Figure 6 (b) shows the difference between the data (symbols) and simulations of the Ising model without (dashed line), and with (solid line at the origin), the nonlinear correction. Indeed, using g=1 with the optimal region size (n=27) reduces the standard deviation by an order of magnitude. Figure 6 (c) shows the effective scaling exponent γ_{eff} as a function of reduced temperature, from the magnitude of the slope when plotted as in Fig. 6 (a). The data (symbols) and simulations with nonlinear correction (solid line) show conspicuous

Figure 6. From Ref. [15]. (**a**) Critical scaling plot of magnetic susceptibility versus reduced temperature, $\tau = (T\text{-}T_C)/T_C$. Symbols are from measurements of gadolinium. Lines are from simulations of the Ising model with (g=1, solid) and without (g=0, dashed) the quadratic correction in Eq. (3). (**b**) Residual plot of the data and g=0 simulations, from g=1 at the origin. (**c**) Effective scaling exponent (magnitude of slope from Fig. 6 (**a**)) for the Gd data and Ising-model simulations.

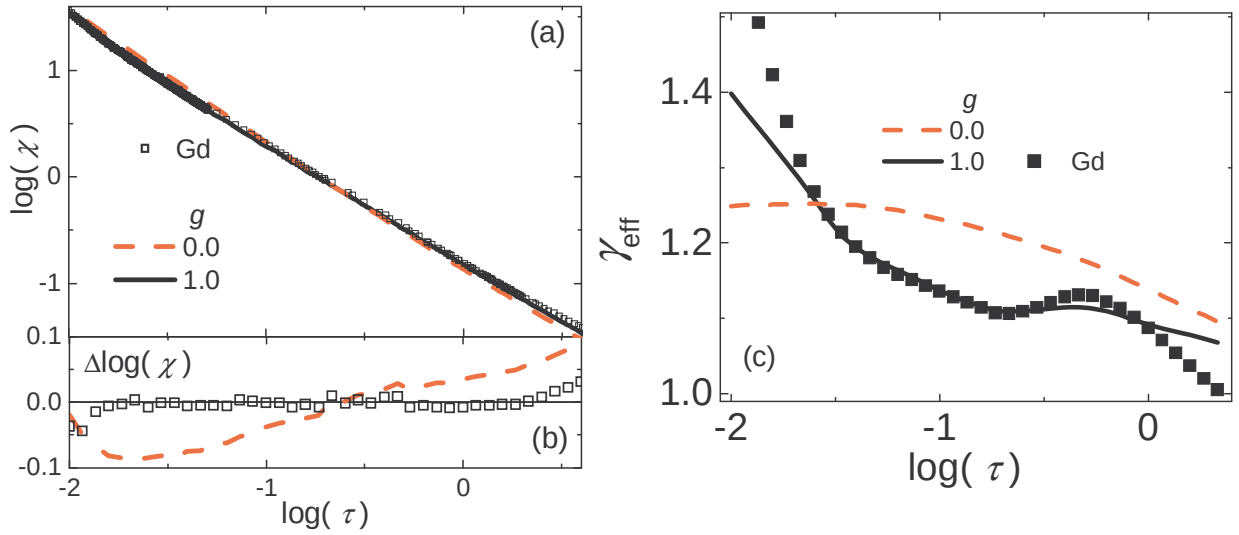

features that clearly differ from the monotonic behavior [34] of simulations using Boltzmann's factor alone (dashed line). In fact, when measured to within 0.01 % of T_C, ultra-high-purity gadolinium crystals show a sharp maximum with $\gamma_{eff} > 1.5$, and $\gamma_{eff} \rightarrow 1$ as $T \rightarrow T_C$ [35], clearly incompatible with the Ising model for homogeneous samples in the canonical ensemble.

The solid line in Fig. 7 shows the excess specific heat measured in the colossal magneto-resistance material $LaMnO_3$. The peak identifies the phase transition from a Jahn-Teller distortion that occurs at $T_c \approx 730$ K. The dashed line comes from simulations of the Ising model using Boltzmann's factor alone (g=0), while the solid symbols come from the same model with the nonlinear correction (g=1 in Eq. (3)) and optimal region size n=27. Again the nonlinear correction gives significantly better agreement with the measured behavior.

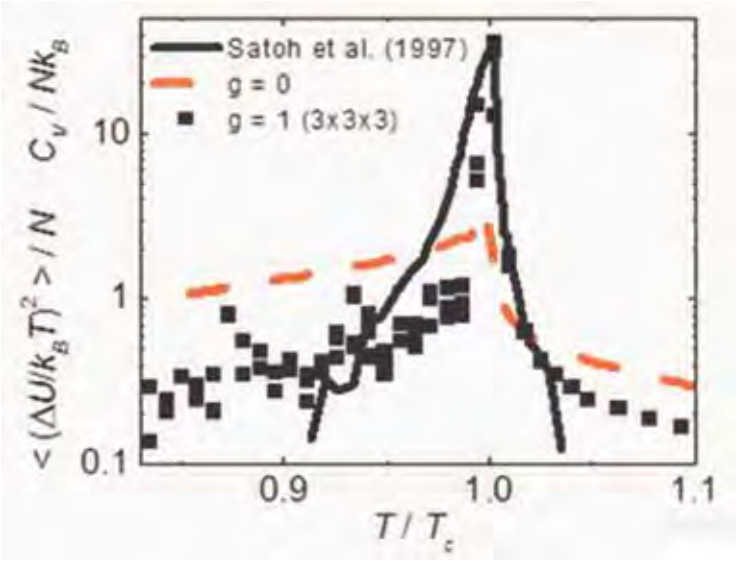

Figure 7. From Ref. [16]. Excess specific heat as a function of normalized temperature. Solid line is from measurements of $LaMnO_3$ near its Jahn-Teller distortion temperature, T_c. Dashed line and symbols come from simulations of the Ising model without (g=0) and with (g=1) the nonlinear correction.

Figure 8. From Refs. [16,37]. Pair distribution functions (PDFs) from neutron scattering in $LaMnO_3$. Upper lines show two PDFs; one from above the Jahn-Teller distortion temperature and one from below, with an identical background removed from both. Lower line shows the difference between these two PDFs. Note the enhanced correlation at short distances, then abrupt loss of correlation at radius $r \approx 1.0$ nm, corresponding to the distance between three lattice sites.

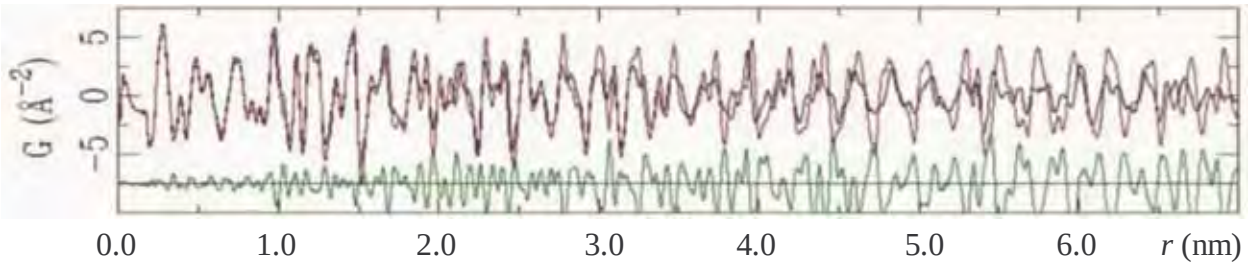

Direct evidence for heterogeneous correlations in crystals of $LaMnO_3$ comes from neutron scattering [36,37]. The upper two lines in Fig. 8 show the pair distribution function (PDF) measured above, and below, the Jahn-Teller transition temperature. The difference between these PDFs (lower curve) shows strong correlations in the positions of neighboring atoms out to a distance of ~1.0 nm, then abrupt loss in correlation beyond [16].

Figure 9 shows the pair-correlation function from simulations of the Ising model without (g=0, dashed lines) and with (g=1, symbols) the nonlinear correction. When g=0 there is a smooth loss in correlation, characteristic of the classical picture. When g=1 there is stronger correlation over the three contiguous lattice sites within each region, then an abrupt loss in correlation to the neighboring region, consistent with the measured pair distribution function shown in the lower part of Fig. 8. The inset of Fig. 9 shows that linear regression on three adjacent sites in a region, from simulations with g=1, yields a correlation length that is similar to the radius of distinct regions deduced from neutron scattering.

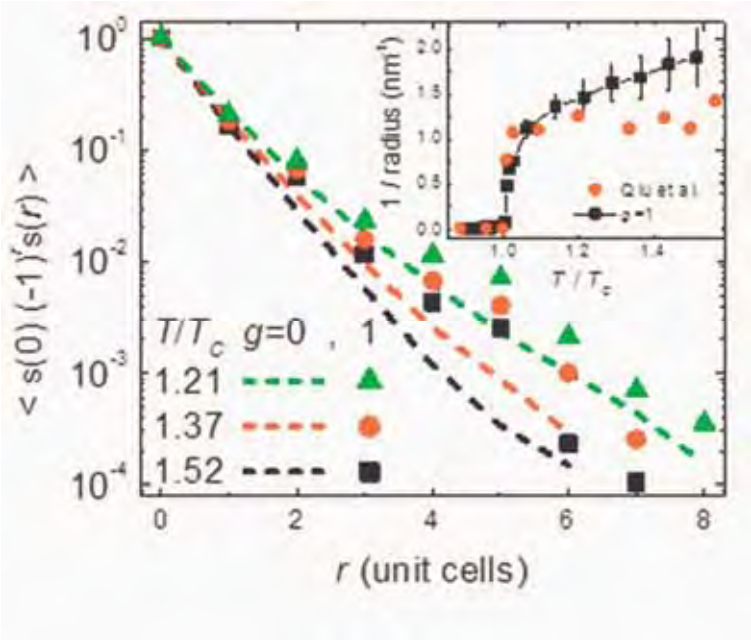

Figure 9. From Refs. [16,37]. Pair correlation function versus distance, from simulations of the Ising model. Dashed lines show smooth loss in correlation when g=0. When g=1, the symbols show an abrupt loss in correlation between regions, with a more-gradual loss beyond the abrupt jump. Strong correlations that persist for three lattice sites are consistent with Fig. 8, and $n = 3^3$ in Fig. 7. This non-monotonic loss in correlation deviates from the classical Ornstein-Zernicke picture [38], where the pair-correlation function is predicted to diminish smoothly and homogeneously around every atom. Thus, the classical picture of homogeneous correlations is invalid on length scales of nanometers, where quantum mechanics may influence the correlations.

Additional direct evidence for heterogeneous correlations comes from multi-dimensional NMR [39,40]. Measurements and analysis yield an average size for the independently relaxing regions of 10, 76, and 390 molecules (or monomer units) in glycerol, ortho-terphenyl, and polyvinyl acetate, respectively. The distribution of relaxation times gives response rates that can vary by several orders of magnitude across nanometer length scales. Nonresonant spectral hole burning measurements indicate that this heterogeneity corresponds to effective local temperatures that also vary between these regions, indicating *thermo*dynamic heterogeneity. Thus, accurate models and theories of nanometer-sized independently-relaxing regions must obey the laws of nanothermodynamics, consistent with improved agreement between computer simulations and measured data shown in Figs. 2, 3, 6, and 7.

5. Simplified Creutz Model for a Finite System with Localized Heat Bath

The Creutz model consists of a binary system coupled to an explicit heat bath [41]. The model has two types of particles: Ising-like "spins" that have fixed positions on a lattice (the system), and kinetic-energy-carrying "demons" that move through the lattice (the heat bath). The demons are Einstein-like oscillators that act as a source of kinetic energy, with energy-level spacing equal to the difference between Ising states, allowing microcanonical simulations where the total energy is exactly conserved at every step. The dynamics of the Creutz model involves choosing a demon, moving it to a neighboring site in a chosen direction, and testing the potential energy of the spin at that site for possible inversion. If the potential energy decreases or stays the same the spin always inverts, giving any extra energy to the demon. If the potential energy tries to increase, the demon must have enough energy to invert the spin without reaching negative kinetic energy. Thus, the standard Creutz model is a type of cellular automata, with dynamics that can be made deterministic [41]. We have investigated a simplified Creutz model, where the local interaction between spins is replaced by a uniform interaction with an external field (B) [42]. Key advantages of the simplified Creutz model are that the exact canonical distributions and entropies are known for both the system and its bath.

The zeroth law of thermodynamics states that when two systems are in thermal equilibrium they have the same temperature, T, but the law does not specify the statistical distribution needed to calculate T. Although many quantized systems can be characterized by Bose-Einstein (BE) or Fermi-Dirac (FD) statistics, these distributions rely on the usual assumptions of Boltzmann's factor [43,15]: the heat bath must be effectively infinite, with weak coupling between the system and its bath, so that adding one unit of energy to the system does not change the probability of adding a second unit. We have explored some consequences of using a finite heat bath, with quantized energies for the system and bath. We find that assuming the BE and FD distributions yields unequal canonical temperatures for the system and its bath. We obtain the spin temperature T_S from the average units of energy per spin m/M, and the demon temperature T_D from the average units of energy per demon n/N. Specifically, T_D is obtained from inverting the BE distribution, $\varepsilon/k_BT_D = \ln[(n+N)/n]$, while T_S is obtained from inverting the FD distribution, $\varepsilon/k_BT_S = \ln[(M-m)/m]$. From computer simulations of the simplified Creutz model we find that

T_D and T_S often differ significantly. One source of this mismatch comes from finite-size effects, as found in simulations and theory of critical clusters during nucleation [44,45]. In the limit of large systems (N~M>>1000) this temperature mismatch goes to zero ($T_D \rightarrow T_S$), as the energy densities approach the canonical BE and FD distributions $n \rightarrow n_0$ and $m \rightarrow m_0$. However, if energy-carrying demons are reflected internally on an intermediate length (IL), the temperature mismatch is independent of system size.

We model this persistent mismatch in canonical temperature using an effective interaction between neighboring quanta of energy, combined with a chemical potential to accommodate conservation of energy. Thus this temperature mismatch can be attributed to correlations between units of energy when energy is quantized and conserved. We have found that this model adjusts the BE and FD distributions to yield a single T, and it provides good agreement with measured excess specific heat from imperfect crystals at low T. The symbols in Fig. 10 come from IL dynamics where energetic demons reflect at boundaries between regions with sides of length L=3 or 4, as given in the figure. Random walk dynamics (RW, not shown in Fig. 10) would yield zero offset as $M \rightarrow \infty$, corresponding to the dot-dashed line at the origin. We emphasize that the maximum deviation from canonical statistics occurs for IL dynamics with L=3, returning to the canonical distributions for short-ranged RW or for long-ranged ballistic motion. This IL scale, larger than atomic spacing but smaller than sample size, may be related to the "universal" mean-free path of acoustic waves in disordered materials [46]. Open triangles show the offset in demon energy $(n–n_0)/N$ as a function of k_BT_D/ε, whereas closed triangles show the offset in spin energy $(m–m_0)/M$ as a function of k_BT_S/ε. Note the conspicuous increase in $(n–n_0)/N$ and shift to higher k_BT_D/ε, while $(m–m_0)/M$ decreases an equal amount (to conserve energy) and shifts to lower k_BT_S/ε. Dotted lines connect symbols from the same simulation at the same total energy. Thus, the horizontal offset between each pair of connected symbols shows the

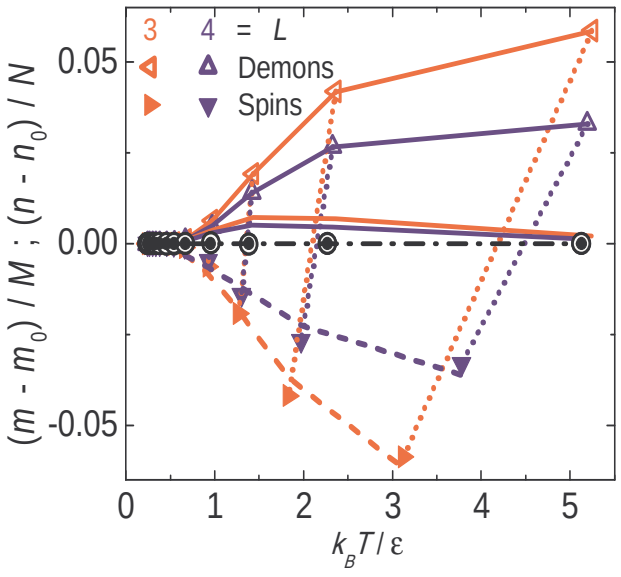

Figure. 10. From reference [42]. Difference between simulated and theoretical energy densities as a function of canonical temperature (triangles) or corrected temperature (circles). Open and solid symbols are from demons and spins, respectively, with symbol shape and color identifying the distance (L) between scattering surfaces for demon motion. Dotted lines connect pairs of points from the same simulation at the same total energy, so that the slope of these lines shows the mismatch in canonical temperature. Note that the increase in demon energy above the center line matches the decrease in spin energy below the line, as required by conservation of energy. Other lines come from various models, as described in the text. Circles show the corrected energy differences at the corrected temperatures for the demons (open circles) and spins (solid circles near the center of the open circles). The dot-dashed line shows zero deviation from the expected energies.

mismatch in temperature, which exceeds 40% for L=3 at the highest energy. Recent results [47] have shown that in fact this mismatch in temperature comes from an inhomogeneous demon density due to the reflection process. Physically the inhomogeneous particle density may come from standing waves, related to the measured "universal" mean-free path of acoustic phonons. In any case, the maximum mismatch in canonical temperature occurs when L=3, where energetic demons are maximally localized to the single site at the center of each 3x3x3 region.

The solid and dashed lines in Fig. 10 come from the BE and FD distributions using the usual Creutz temperature, $\varepsilon/k_BT_D = \ln[(n_0+N)/n_0]$. Specifically, the upper two solid lines show the BE distribution as a function of T_D, $1/(e^{\varepsilon/k_BT_D}-1) - n_0/N$, which agrees with simulations of $(n-n_0)/N$ exactly by definition of T_D. The other two solid lines show that the FD distribution as a function of T_D, $1/(e^{\varepsilon/k_BT_D}+1) - m_0/M$, has a small increase in energy, opposite to the decrease required by conservation of energy and shown by the simulations. The dashed lines that roughly follow the lower two sets of symbols again use T_D in the FD function, but with the numerator and energy spacing adjusted to best fit the data, then plotted as a function of T_S. For L=3, the fit parameter ε=1.93±0.02 differs from the actual energy spacing ε=2, while the numerator 0.835±0.005 also differs significantly from its actual value of 1. Similarly, some values of this FD function differ from the simulation values of m/M by more than 10 standard deviations. Thus, for IL dynamics, the energies cannot be described by the BE and FD distributions alone.

To characterize deviations from the canonical distributions we use an interacting lattice-gas model for adsorption of particles on neighboring sites [48], adapted to treat quanta of energy. We find that the offset in canonical temperatures can be modeled by an effective potential w<0, which causes a correlation between energy quanta on neighboring sites. Although agreement with simulations may be better if all possible arrangements of occupied sites in a region are included, here for simplicity we consider only nearest-neighbor pairs. The partition function is: $\xi = 1+2ae^{-\varepsilon/k_BT_{RW}} + a^2e^{-2\varepsilon/k_BT_{RW}}e^{-w/k_BT_{RW}}$, where $a=e^{\mu/k_BT_{RW}}$ is the energy-quantum activity at the canonical (random-walk) temperature T_{RW}, with μ the chemical potential. The three terms in ξ come from: no units of energy, one unit of energy on either site, and one unit of energy on both sites, which includes the effective interaction potential. The probability of finding no energy on either site is $1/\xi$. Using conservation of total energy, the density of energy in demons and spins becomes $n/N = n_0/N + A/\xi$ and $m/M = m_0/M - A/\xi$, respectively. Here we use A as an adjustable parameter that governs the strength of the energy transfer mechanism. We also adjust a to the best value for each set of simulations. A consistent equilibrium temperature is obtained by inverting either energy density, with the appropriate offset: $\varepsilon/k_BT = \ln[1/(n/N-A/\xi)+1]$ or $\varepsilon/k_BT = \ln[1/(m/N+A/\xi)-1]$. The open circles in Fig. 10, with solid circles near their centers, show that the corrected BE and FD distributions give good agreement with the energies of the demons and spins, and equilibrium temperatures that match.

Heat capacity in the standard Debye model is proportional to the size of the lattice, so that at low temperature it can be written as $C_D = DMT^3$. Here D is a constant that depends on the number of degrees of freedom per lattice site. To characterize measured excess specific heat we assume that any extra energy adsorbed on a lattice site simply adds to its degrees of freedom, so

that $D \rightarrow D + C(\bar{\varepsilon}/\varepsilon)(m - m_0)/(MA)$. Here C is an excess specific heat constant, $(m - m_0)$ gives the additional units of energy at each site, $\bar{\varepsilon} = k_B T^2 \, \partial \ln(\xi)/\partial T$ is the average energy from the adsorption model, and the ratio $\bar{\varepsilon}/\varepsilon$ may be a simplistic way to count the extra units of energy when ε comes from a distribution. The modified and normalized specific heat can be written as:

$$C_a / (MT^3) = D - C[2ae^{-\varepsilon/k_B T} + (2 + w/\varepsilon)\, a^2 e^{-2\varepsilon/k_B T} e^{-w/k_B T}] / \xi^2 \qquad (4)$$

Note that because $(2 + w/\varepsilon) < 0$, the quantity in square brackets is often negative, yielding excess specific heat for $C > 0$.

Symbols in Fig. 11 show the measured excess specific heat reported in the literature for three different crystalline substances. Solid curves are the best fits to these data using Eq. (4). Despite the simplistic way that Einstein-like oscillators are added to Debye-like vibrations, Eq. (4) gives good agreement with the excess specific heat in these samples. In the Creutz model, equal energy spacing simplifies the simulations and facilitates conservation of energy. From the measured excess specific heat of imperfect crystals, agreement with the model using equal energy spacing could indicate a type of resonance, or other inherent connection between phonon localization and the two-level systems [49].

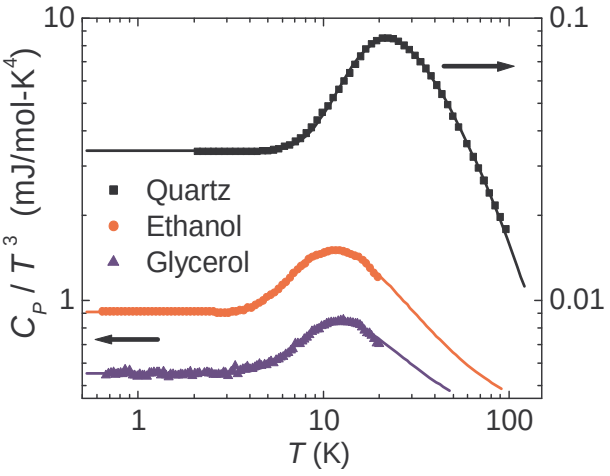

Figure. 11. From reference [42]. Normalized specific heat as a function of temperature on a log-log plot. Symbols come from the measured specific heat of three different crystalline substances: quartz (black squares), ethanol (red circles), and glycerol (blue triangles). Debye theory predicts constant values of C_P/T^3 at these low temperatures, as seen below 3 K. Solid lines come from best fits to the excess specific heat that peaks above 10 K using Eq. (1) as described in the text. Agreement with the data suggests that the excess specific heat comes from extra units of energy that are adsorbed on the lattice due to an effective interaction between energy units on neighboring sites.

6. Magnetoresistance in Nickel-Silicide Nanowires from Nonequilibrium Heating

When subjected to a changing magnetic field, the low-temperature resistance of Ni-Si nanowires can change by a factor of two or more [50-53]. Furthermore, this magnetoresistance shows strong hysteresis as a function of field, and slow relaxation as a function of time. We model this behavior assuming adiabatic demagnetization of magnetic spins, with charge carriers that are also weakly coupled to the thermal bath.

To quantify the weak thermal link we calculate the local temperature and its change relative to the bulk temperature: $\Delta T \equiv T_L - T^*$. For adiabatic spins, thermodynamic principles [54] predict that changes in temperature are proportional to the temperature-dependent slope of the magnetic moment $(\partial M/\partial T_L)_H$ divided by the heat capacity at constant pressure c_p. We obtain expressions

for the change in temperature as a function of time while the field is changing $t \le t_{fin}$, and after the field sweep is stopped $t \ge t_{fin}$:

$$\Delta T = \alpha r \tau \left(1 - e^{-t/\tau}\right) \qquad t \le t_{fin}, \tag{5a}$$

$$\Delta T = \alpha r \tau \left(e^{t_{fin}/\tau} - 1\right) e^{-t/\tau} \qquad t \ge t_{fin}. \tag{5b}$$

Here r is the field sweep rate, α is an amplitude factor, and τ is the time constant for coupling to the thermal bath. Some results using this model are shown in Fig. 12.

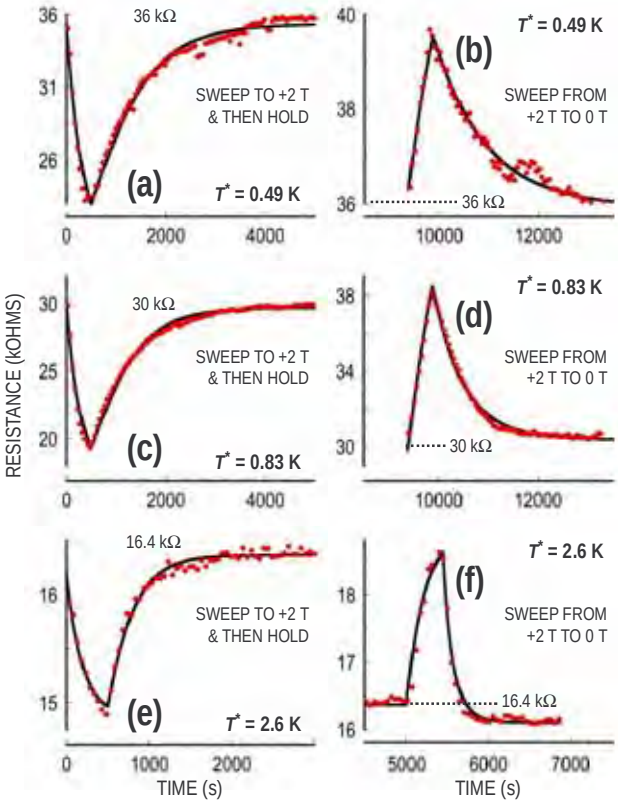

Figure 12. From reference [53]**.** Two-stage magneto-resistance relaxation measurements. Panels (a), (c) & (e) were obtained by sweeping the field from zero to +2 T, and then holding at +2 T. Subsequently, panels (b), (d) & (f) were obtained after allowing the sample to equilibrate for a long time (as indicated by the offset in the time axis), before sweeping the field down from +2 T to zero. In each of the panels the gray region denotes the interval over which the magnetic field was swept. Field sweep rates are 0.2 T/min in each of the panels, with the sample temperature (T^*) as indicated. Solid curves through the data represent fits from Eqs. 5a and 5b.

7. Deviations from the Equipartition Theorem in Simulations of Simple Fluids

Figure 13 shows size-dependent fluctuations in kinetic energy, normalized by a formula that would yield zero if the system obeyed the equipartition theorem. The data (symbols) are from microcanonical molecular dynamics (MD) simulations of systems with four different particle densities, using a Lennard-Jones (L-J) interaction, with the same potential-energy minimum ε for all systems. The symbols come from averaging the behavior at three temperatures kT/ε = 0.01, 0.02, and 0.05, with error bars from the standard deviation. When properly normalized by $kT/n\varepsilon$, these fluctuations exceed the equipartition theorem by at least a factor of ten. For all systems, the deviations per particle decrease with increasing system size, consistent with a surface term that varies as $n^{2/3}/n$ (dashed lines) that goes to zero in the thermodynamic limit. However, for finite systems these size dependent fluctuations cause the local entropy to be non-extensive and non-additive, deviating from standard thermodynamic behavior, and disagreeing with measurements that show constant specific heat for independent fluctuations inside bulk materials.

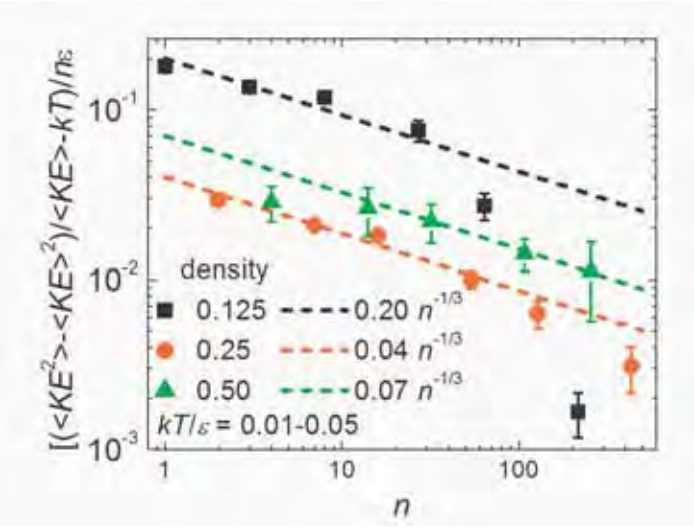

Figure 13. (unpublished) Normalized fluctuations in kinetic energy as a function of the number of particles in the region, from MD simulations of the Lennard-Jones model.

Deviations from standard thermodynamics shown by computer simulations arise from assuming homogeneous correlations between particles. Specifically, when energy fluctuations are averaged over a volume that excludes interacting particles outside the volume, correlations that influence the energy fluctuations are neglected. However, several experimental techniques have shown that primary response usually comes from an ensemble of independently-relaxing nanometer-sized regions, establishing that correlations between neighboring particles in most materials are heterogeneous. Indeed, many measurements have found that heterogeneity dominates the response of liquids, glasses, polymers, and crystals [55-58]. In fact, detailed studies of time-dependent specific heat at low temperatures find that only one substance agrees fully with the Debye T^3 law: chemically and isotopically pure NaF crystals [59]. Furthermore, results from the technique of nonresonant spectral hole burning (NSHB) indicate that specific heat is constant for independently relaxing regions inside bulk samples [60], even for regions having n<10 molecules [61]. Thus, the primary response in most materials is dominated by heterogeneous correlations, different from the behavior shown by standard MD simulations.

8. Discussion

Some remarkably universal empirical formulas are often used to characterize the measured response from many materials. For example, many materials that exhibit non-Nyquist noise have been characterized by a frequency dependence $1/f^{\alpha}$ with $\alpha \sim 1$, as shown in Figs. 2 and 3. Non-classical critical scaling has been used for behavior near phase transitions, as shown in Fig. 6. Two-level systems of uncertain origin have been used for the excess specific heat and time-dependent behavior at low temperatures, as shown in Figs. 11-12. In many cases these expressions are convenient mathematical formulas for cataloging the measured response of complex systems, but data of sufficient quality over broad enough range invariably show deviations from these formulas. Many models have been proposed for each of the empirical formulas, so that the deviations may be a decisive way to distinguish between models. The nonlinear correction to Boltzmann's factor provides a common foundation for all of these formulas, including many of the measured deviations. Moreover, the correction is necessary to describe the thermal equilibrium of any sample that contains independently fluctuating regions if the fluctuations themselves are to govern the distribution of region sizes.

Standard models based on homogeneous thermodynamics have been unable to explain several features in the dynamics of complex systems. The deviations may be quite subtle. Indeed, it can be difficult to see curvature in the data on a log-log critical-scaling plot, as shown in Fig. 6 (a). Nevertheless, other researchers have also recognized that most ferromagnetic materials deviate from standard critical-scaling behavior. In 1989 Collins wrote [62]: "The critical exponents of iron and nickel are very similar to each other, while those for cobalt are clearly different. There is no theoretical understanding of these results." Also in 1989 Hohenemser et al. wrote [63]: "At the same time our review makes clear that when one restricts the analysis to the best experiments, only a few materials correspond unambiguously to these models, while most do not." In fact, by plotting the residuals (as in Fig. 6 (b)) the nonlinear correction clearly improves the agreement between the Ising model and measurements. Moreover, the monotonic behavior of standard simulations of the Ising model cannot match the sharp temperature-dependent features in the effective scaling exponent, as shown in Fig. 6 (c). In any case, such nonlinear corrections are necessary if independently-fluctuating nanometer-sized regions inside bulk samples are to strictly conserve total energy and maintain maximum entropy during equilibrium fluctuations.

9. Conclusions

We have shown that nonlinear corrections in thermodynamics provide fundamental insight into the local dynamics inside complex materials. Although full understanding of all features will require sophisticated studies, even the most-simplistic models can match measured behavior when appropriate nonlinear corrections are used, as shown in Figs. 2, 3, 6, 7, 9, and 11. From the discussion around Fig. 4 it is possible to emphasize the following results regarding the laws of nanothermodynamics. The 1st law requires that total energy is strictly conserved at all times, including Hill's subdivision potential from the configurational entropy when localized regions fluctuate. The 2nd law requires that the entropy of an isolated system must never decrease, so that if a local region fluctuates into a low-entropy state, the entropy of its thermal bath must increase to compensate. Thus, the nonlinear corrections extend standard thermodynamics to treat finite-size fluctuations, while strictly maintaining the fundamental laws of physics. Moreover, these corrections yield the statistics of indistinguishable particles within each region, as is needed to avoid non-extensive entropy, resolve Gibbs' paradox, and mimic quantum-mechanical behavior for fundamental particles in nanometer-sized regions, as discussed in connection with Figs. 4 and 5. Indeed, the cooperative dynamics within each region and uncorrelated dynamics between neighboring regions, combined with the fact that standard thermodynamics accurately describes macroscopic coherent states, suggests a connection to quantum mechanics [64,65]. Specifically, each region may be associated with localized excitations that have phase incoherence with excitations in neighboring regions, so that the nonlinear corrections provide a fundamental connection between quantum mechanics on the scale of nanometers and the bulk behavior of complex materials. Similar multi-scale modeling and quantum-based calculations are crucial for accurate simulations of energetic materials [66-68]. This combination of large-scale quantum behavior with small-system thermodynamics is the main focus of our current research.

Bibliography

1 Much of this report is based on the review article: Chamberlin, R.V., The big world of nanothermodynamics, *Entropy* **2015**, *17*, 52-73

2 Hill, T.L., Thermodynamics of small systems, *J. Chem. Phys.* **1962**, *36*, 3182-3197

3 Hill, T.L., *Thermodynamics of Small Systems*, Parts I & II, Dover Publications, Mineola, NY, **2013**

4 Donth, E., The size of cooperatively rearranging regions at the glass transition, *J. Non-Cryst. Solids* **1982**, *53*, 325-330

5 Yukalov, V.I., Phase transitions and heterophase fluctuations, *Phys. Rep.* **1991**, *208*, 395-489

6 Chamberlin, R.V., Experiments and theory of the nonexponential relaxation in liquids, glasses, polymers and crystals, *Phase Transitions* **1998**, *65*, 169-209

7 Böhmer, R.; Chamberlin, R.V.; Diezemann, G.; Geil, B.; Heuer, A.; Hinze, G.; Kuebler, S.C.; Richert, R.; Schiener, B.; Sillescu, H.; Spiess, H.W.; Tracht, U.; Wilhelm, M., Nature of the non-exponential primary relaxation in structural glass-formers probed by dynamically selective experiments, *J. Non-Cryst. Solids* **1998**, *235-237*, 1-9

8 Ediger, M.D., Spatially heterogeneous dynamics in supercooled liquids, *Annu. Rev. Phys. Chem.* **2000**, *51*, 99-128

9 Richert, R., Heterogeneous dynamics in liquids: fluctuations in space and time, *J. Phys. Condens. Matter* **2002**, *14*, R703-R738

10 Hill, T.L., A different approach to nanothermodynamics, *Nano Lett.* **2001**, *1*, 273-275

11 Chamberlin, R.V., Mesoscopic mean-field theory for supercooled liquids and the glass transition, *Phys. Rev. Lett.* **1999**, *82*, 2520-2523

12 Chamberlin, R.V., Critical behavior from Landau theory in nanothermodynamic equilibrium, *Phys. Lett. A* **2003**, *315*, 313-318

13 Javaheri, M.R.H.; Chamberlin, R.V., A free-energy landscape picture and Landau theory for the dynamics of disordered materials, *J. Chem. Phys.* **2006**, *125*, 154503

14 Chamberlin, R.V.; Wolf, G.H., Fluctuation-theory constraint for extensive entropy in Monte-Carlo simulations, *Eur. Phys. J. B* **2009**, *67*, 495-499

15 Chamberlin, R.V.; Vermaas, J.V.; Wolf, G.H., Beyond the Boltzmann factor for corrections to scaling in ferromagnetic materials and critical fluids, *Eur. Phys. J. B* **2009**, *71*, 1-6

16 Chamberlin, R.V., Monte Carlo simulations including energy from an entropic force, *Physica A* **2012**, *391*, 5384-5391

17 Chamberlin R.V.; Nasir, D.M., 1/*f* noise from the laws of thermodynamics for finite-size fluctuations, *Phys. Rev. E* **2014**, *90*, 012142

18 Kogan, S. *Electronic noise and fluctuations in solids*, Cambridge Univ. Press, Cambridge, **2008**

19 Dutta, P.; Horn, P.M., Low-frequency fluctuations in solids: 1/*f* noise, *Rev. Mod. Phys.* **1981**, *53*, 497-516

20 Weissman, M.B., 1/*f* noise and other slow, nonexponential kinetics in condensed matter, *Rev. Mod. Phys.* **1988**, *60*, 537-571

21 Milotti, E., 1/*f* noise: a pedagogical review, Arxiv preprint physics/0204033 **2002** archiv.org

22 Paladin, E.; Galperin, Y.M.; Falci, G.; Altshuler, B.L., 1/*f* noise: Implications for solid-state quantum information, *Rev. Mod. Phys.* **2014**, *86*, 361-418

23 Voss, R.F.; Clarke, J., '1/*f* noise' in music and speech, *Nature* **1975**, *258*, 317-318

24 West, B.J.; Shlesinger, M., The noise in natural phenomena, *Amer. Sci.* **1990**, *78*, 40-45

25 Stanley, H.E.; Buldyrev, S.V.; Goldberger, Z.D.; Havlin, S.; Mantegna, R.N.; Ossadnik, S.M.; Peng, C.K.; Simons, M., Statistical mechanics in biology: how ubiquitous are long-range correlations?, *Physica A* **1994**, *78*, 214-253

26 Gilden, D.L.; Thornton, T.; Mallon, M.W., 1/*f* noise in human cognition, *Science* **1995**, *267*, 1837-1839

27 Wang, G.M.; Sevick, E.M.; Mittag, E.; Searles, D.J.; Evans, D.J., Experimental demonstration of violations of the second law of thermodynamics for small systems and short time scales, *Phys. Rev. Lett.* **2002**, *89*, 050601

28 Sampat, N.; Meissner, M., Time-dependent specific heat of crystals and glasses at low temperatures, In *Die Kunst of Phonons*, eds. T. Paszkiewicz and K. Rapcewicz, Springer Verlag, 1994; pp. 105-112.

29 Schiener, B.; Böhmer, R.; Loidl, A.; Chamberlin, R.V., Nonresonant spectral hole burning in the slow dielectric response of supercooled liquids, *Science*, **1996**, *274*, 752-754

30 Chamberlin, R.V., Nonresonant spectral hole burning in a spin glass, *Phys. Rev. Lett.* **1999**, *83*, 5134-5137

31 Binder, K., Finite size scaling analysis of Ising model block distribution functions, *Z. Phys. B* **1981**, *43*, 119-140

32 Duvvuri, K.; Richert, R., Dielectric hole burning in the high frequency wing of supercooled glycerol, *J. Chem. Phys.* **2002**, *118*, 1356-1363

33 Reinsberg, S.A.; Heuer, A.; Doliwa, B.; Zimmermann, H.; Spiess, H.W., Comparative study of the NMR length scale of dynamic heterogeneities of three different glass formers, *J. Non-Cryst. Solids* **2002**, *307-310*, 208-214

34 Luijten, E.; Binder, K., Nature of crossover from classical to Ising-like critical scaling behavior, *Phys. Rev. E* **1998**, *58*, R4060-R4063

35 Srinath, S.; Kaul, S.N.; Kronmüller, H., Observation of isotropic dipolar to uniaxial dipolar crossover in gadolinium, *Phys. Rev. B* **1999**, *59*, 1145-1151

36 Billinge, S.J.L., Nanoscale structural order from the atomic pair distribution function (PDF): There's plenty of room in the middle, *J. Sol. St. Chem.* **2008**, *181*, 1695-1700

37 Qiu, X.; Proffen, T.; Mitchell, J.F.; Billinge, S.J.L., Orbital correlations in the pseudocubic *O* and rhombohedral *R* phases of LaMnO3, *Phys. Rev. Lett.* **2005**, *94*, 177203

38 Ornstein, L.S.; Zernike, F., Accidental deviations of density and opalescence at the critical point of a single substance, *Proc. Acad. Sci. Amsterdam* **1914**, *17*, 793-806

39 Schmidt-Rohr, K.; Spiess, H.W., Nature of nonexponential loss of correlation above the glass transition investigated by multidimensional NMR, *Phys. Rev. Lett.* **1991**, *66*, 3020-3023

40 Tracht, U.; Wilhelm, M.; Heuer, A.; Schmidt-Rohr, K.; Spiess, H.W., Length scale of dynamic heterogeneities at the glass transition determined by multidimensional nuclear magnetic resonance, *Phys. Rev. Lett.* **1998**, *81*, 2727-2730

41 Creutz, M., Deterministic Ising dynamics, *Ann. Phys.* **1986**, *167*, 62-72

42 Chamberlin, R.V.; Davis, B.F., Modified Bose-Einstein and Fermi-Dirac statistics if excitations are localized on an intermediate length scale: Applications to non-Deby specific heat, *Phys. Rev. E* **2013** *88*, 042108

43 Feynman, R.P., *Statistical Mechanics* (Perseus, Reading, MA, 1998) Chapt. 1.

44 Wedekind, J.; Reguera, D.; Strey, R., Influence of thermostats and carrier gas on simulations of nucleation, *J. Chem. Phys.* **2007**, *127*, 064501

45 Schmelzer, J.W.P.; Boltachev, G.S.; Abyzov, S.S., Temperature of critical clusters in nucleation theory: Generalized Gibbs‘ approach, *J. Chem. Phys.* **2013**, *139*, 034702

46 Foret, M.; Courtens, E.; Vacher, R.; Suck, J.B., Scattering investigation of acoustic localization in fused silica, *Phys. Rev. Lett.* **1996**, *77*, 3831-3834

47 Moffet, S., unpublished.

48 Hill, T.L., *An Introduction to Statistical Thermodynamics* (Dover, New York, 1986) pg. 133.

49 Schroeder, J.; Wu, W.; Apkarian, J.L.; Lee, M.; Hwa, L.G.; Moynihan, C.T., Raman scattering and boson peaks in glasses: temperature and pressure effects, *J. Non-Cryst. Sol.* **2004**, *349*, 88-97

50 Seo, K.; Varadwaj, K.S.K.; Mohanty, P.; Lee, S.; Jo, Y.; Jung, M.H.; Kim, J.; Kim, B., Magnetic properties of single-crystalline CoSi nanowires, *Nano Lett.* **2007**, *7*, 1240-1245

51 Kim, T.; Naser, B.; Chamberlin, R.V.; Schilfgaarde, M.V.; Bennett, P.A.; Bird, J.P., Large hysteretic magnetoresistance of silicide nanostructures, *Phys. Rev. B.* **2007**, *76*, 184404

52 Kim, T.; Chamberlin, R.V.; Bennett, P.A.; Bird, J. P., Dynamical characteristics of the giant magnetoresistance of epitaxial silicide nanowires, *Nanotechnol*. **2009**, *20*, 135401

53 Kim, T.; Chamberlin, R.V.; Bird, J.P., Large magnetoresistance of nickel-silicide nanowires: Equilibrium heating and magnetically-coupled dangling bonds, *Nano Lett*. **2013**, *13*, 1106-1110

54 Kunzler, J.E.; Walker, L.R.; Galt, J.K., Adiabatic demagnetization and specific heat in ferrimagnets, *Phys. Rev*. **1960**, *119*, 1609-1614

55 Chamberlin, R.V., Experiments and theory of the nonexponential relaxation in liquids, glasses, polymers and crystals, *Phase Transitions* **1998**, *65*, 169-209

56 Böhmer, R.; Chamberlin, R.V.; Diezemann, G.; Geil, B.; Heuer, A.; Hinze, G.; Kuebler, S.C.; Richert, R.; Schiener, B.; Sillescu, H.; Spiess, H.W.; Tracht, U.; Wilhelm, M., Nature of the non-exponential primary relaxation in structural glass-formers probed by dynamically selective experiments, *J. Non-Cryst. Solids* **1998**, *235-237*, 1-9

57 Ediger, M.D., Spatially heterogeneous dynamics in supercooled liquids, *Annu. Rev. Phys. Chem.* **2000**, *51*, 99-128

58 Richert, R., Heterogeneous dynamics in liquids: fluctuations in space and time, *J. Phys. Condens. Matter* **2002**, *14*, R703-R738

59 Sampat, N.; Meissner, M., Time-dependent specific heat of crystals and glasses at low temperatures, pgs. 105-112 in *Die Kunst of Phonons*, eds. T. Paszkiewicz and K. Rapcewicz, Springer Verlag, Berlin, **1994**

60 Duvvuri, K.; Richert, R., Dielectric hole burning in the high frequency wing of supercooled glycerol, *J. Chem. Phys.* **2002**, *118*, 1356-1363

61 Reinsberg, S.A.; Heuer, A.; Doliwa, B.; Zimmermann, H.; Spiess, H.W., Comparative study of the NMR length scale of dynamic heterogeneities of three different glass formers, *J. Non-Cryst. Solids* **2002**, *307-310*, 208-214

62 Collins, M.F., *Magnetic critical scattering*, Oxford Univ. Press, New York 1989

63 Hohenemser, C.; Rosov, N.; Kleinhammes, A., Critical phenomena studied via nuclear techniques, *Hyperfine Interactions*, **1989**, *49*, 267-324

64 Gemmer, J.; Michel, M.; Mahler, G., *Quantum thermodynamics*, 2nd ed., Springer Verlag, Berlin, **2009**

65 Yukalov, V.I., Equilibration and thermalization in finite quantum systems, *Laser Phys. Lett.* **2011**, *8*, 485-507

66 Izvekov, S.; Chung, P.W; Rice, B.M., The multiscale coarse-graining method: Assessing its accuracy and introducing density dependent coarse-grain potentials, *J. Chem. Phys.* **2010**, *133*, 064109

67 Izvekov, S.; Rice, B.M., Multi-scale coarse-graining of non-conservative interactions in molecular liquids, *J. Chem. Phys.* **2014**, *140*, 104104

68 Taylor, D.E.; Rice, B.M., Quantum-informed multiscale M&S for energetic materials, *Adv. Quantum Chem.* **2014,** *69*, 171-219